Electrochimica Acta 105 (2013) 665–670

Contents lists available at SciVerse ScienceDirect

Electrochimica Acta

journal homepage: www.elsevier.com/locate/electacta

A study on the key factors affecting the sensibility of bismuth deposits toward Sn^{2+}: Effects of bismuth microstructures on the Sn^{2+} pre-deposition

Chien-Hung Lien, Chi-Chang Hu*,[1], Kuo-Hsin Chang[1], Yi-Da Tsai, David Shan-Hill Wang

Department of Chemical Engineering, National Tsing Hua University, 101, Section 2, Kuang-Fu Road, Hsin-Chu 30013, Taiwan

ARTICLE INFO

Article history:
Received 12 January 2013
Received in revised form 6 March 2013
Accepted 23 April 2013
Available online xxx

Keywords:
Bismuth-film electrode
Sn^{2+} sensing
Preferred orientation ratio
Grain size
Stripping

ABSTRACT

The pre-deposition of Sn following with the square-wave anodic stripping voltammetric (SWASV) analysis is employed to determine the Sn^{2+}-sensing ability of bismuth-film electrodes (BFEs). The influences of Bi microstructures, such as grain size, preferred orientation ratio between Bi(1 1 0) and Bi(0 1 2) (denoted as *f*), and average roughness factor (Ra) of Bi deposits on the Sn^{2+}-sensing ability, are investigated. The preferred orientation ratio is a key factor determining the Sn^{2+}-sensing ability of BFEs meanwhile a synergistic effect between grain size and *f* on enhancing the current density of Sn^{2+} sensing is obtained when *f* is above 0.11. The crystalline facet of Bi(1 1 0) favorable for pre-depositing Sn is the main reason enhancing the Sn^{2+} sensing of Bi deposits. Thus, this work shows that Sn^{2+} sensing through stripping of pre-deposited Sn on BFEs does not follow the mechanism of forming Bi-alloy amalgams since the successful pre-deposition of trace Sn^{2+} on Bi strongly depends on the effective exposure of crystalline facet of Bi(1 1 0).

1. Introduction

Mercury-film electrodes (MFEs) generally show unique sensing performances in detecting heavy metals in electroanalysis because of the high overpotential of hydrogen evolution [1,2] and the facile formation of amalgams (Hg alloys [3]). However, due to the toxicity of mercury [4], bismuth, a new electrode material, was proposed to be a promising alternative (e.g., bismuth-film electrodes, BFEs) to replace MFEs in 2000 [5]. The widely accepted mechanism for heavy metal-ion sensing on Bi is due to its similar properties in forming fused alloys with heavy metals in comparison with Hg in the simultaneous electrowinning of Bi and heavy metals, then, the detecting process [6–8].

In general, there are three strategies in preparing bismuth electrodes for heavy-metal ion sensing: (1) pre-plating of Bi metal, (2) simultaneous electrowinning of Bi and heavy metal ions, and (3) inserting a Bi precursor into the matrix of electrode materials (e.g., Bi_2O_3 in carbons [9]). The simultaneous electrowinning of Bi and heavy metal ions as well as inserting Bi precursors into the matrix of electrode materials is generally favorable for the amalgam formation of Bi alloys but shows the disadvantages of increasing the complexity of analytes and the coating issues when consumers use such electrodes in detecting real samples [8]. Moreover, since the difference in the equilibrium deposition potentials between Bi and Sn is very large (ca. 0.454 V) [10], effectively simultaneous electrowinning of Bi and Sn ions for Sn^{2+} sensing is still a challenge although a few researches tried to circumvent this issue by using high concentrations of supporting electrolytes [11,12] or adding complexing agents [13–15].

Based on the above considerations, this work focuses on developing BFEs with metallic Bi pre-plated onto the electrode for detecting Sn^{2+} in the media with a low concentration of supporting electrolytes. Here, Sn^{2+}-sensing is employed as the model test because Sn and Sn-based alloys are widely used in advanced package of electronics and semiconductors as well as the food industry. For example, the total amount of food packaging every year is approximately 80,000 million cans [16], meanwhile Sn ions have also been found to be one of the essential trace elements in various metabolic processes of plants, animals and humans. However, tin and its compounds can be leached and thus enter the food chain as inorganic tin or organic tin species [16,17] which have been recognized as toxic compounds to mammals [17]. Hence, Sn-ion sensing will be analyzed by using the anodic stripping voltammetric (ASV) analysis on BFEs [11].

The possible sensing mechanisms of heavy-metal ions on metallic Bi are not described clearly [12,18,19]. Several factors, such as complex agents (e.g., catechol and dimethylglyoxime) [4,20], modified agents (e.g., Nafion, and ionophore–Nafion) [21,22], surface

* Corresponding author at: Department of Chemical Engineering, National Tisng Hua University, Hsin-Chu 30013, Taiwan. Tel.: +886 3 5736027; fax: +886 3 5736027.
E-mail address: cchu@che.nthu.edu.tw (C.-C. Hu).
[1] ISE member.

0013-4686/$ – see front matter © 2013 Elsevier Ltd. All rights reserved.
http://dx.doi.org/10.1016/j.electacta.2013.04.121

roughness [23], substrate [24], morphology [25], grain size [26], etc., were proposed to influence the heavy-metal-ion sensing ability of BFEs. These findings suggest the important but complicated influences of Bi microstructures although there is no systematic comparison of these factors in this field. Based on the above understanding, this work tries to find the key microstructure factors influencing the tin-ion sensing ability of metallic Bi films through a systematic comparison of the grain size, preferred orientation ratio, and roughness factor of Bi deposits. In addition, a mechanism, different from the formation of Bi alloy amalgams, for tin-ion sensing on metallic bismuth is proposed.

2. Experimental

Bismuth deposits were electroplated from a solution containing 0.06 M $Bi(NO_3)_3{\cdot}5H_2O$ (Hayashi, Extra Pure (EP)), 0.3 M citric acid (CA, Shimakyu, EP), 4000 ppm gelatin (from porcine skin, Type A~300 Bloom (G2500-100G)), 0.3 M ethylenediaminetetra-acetic acid (EDTA, Riedel-deHaen, Guarantee Analysis (GA)), and variable concentrations of polyethylene glycol (PEG, MW400, Shimakyu, EP) onto copper substrates (for sensor: 90 circular plates (99.5%) with individual geometric area of 1.094×10^{-2} cm^2 and 1.18×10^{-1} cm in diameter were employed for depositing Bi; for AFM, XRD, and SEM analyses: Cu plates of 1 cm^2 were prepared) which have been deposited with a nickel film (ca. 2 μm). The pretreatment procedures of Cu/Ni substrates completely followed our previous work [26,27]. The Cu/Ni substrates, rinsed with deionized water, were placed in a 50 ml jacket cell and faced with a dimensionally stable anode (DSA) to electroplate Bi deposits. The dimensions of the stirring bar are 1.5 cm in length and 6 mm in diameter. The dimensions of 50 ml jacket cell are 4.5 cm in diameter and 4 cm in height. The pH of plating baths was adjusted with concentrated HCl or NH_4OH. After deposition, these electrodes were repeatedly rinsed with deionized water and finally dried in a vacuum oven at room temperature.

The electrochemical analyses were performed with an electrochemical analyzer system, CHI 663a (CH Instruments, USA). All electrochemical analyses were carried out in a three-compartment cell. An Ag/AgCl electrode (Argenthal, 3 M KCl, 0.207 V versus a standard hydrogen electrode (SHE) at 25 °C) was utilized as the reference electrode and a wound platinum wire served as the counter electrode. For the SWASV measurements, the testing solutions contain 0.1 M CA (Shimakyu, EP) and $SnCl_2{\cdot}nH_2O$ (Hayashi, EP) in variable concentrations. According to our previous study [28], Sn^{2+} in the testing media can be stabilized by concentrated CA to form the Sn^{2+}–CA complexes. The concentrations of Sn(II) ions have been confirmed by an inductively coupled plasma-mass spectrometer (ICP-MS, SCIEX ELAN 5000). The potential for pre-depositing Sn onto the BFEs was fixed at −0.8 V for 300 s under a magnetic stirring rate of 100 rpm. The Sn-coated BFEs rinsed with deionized water were anodically stripped in a 0.1 M CA solution (pH = 2) without stirring. The SWASV curves were recorded between -0.7 and -0.3 V at an applied frequency of 15 Hz with the amplitude of 25 mV and a potential step of 4 mV. All solutions were prepared with deionized water produced by a reagent water system (Milli-Q SP, Japan) at 18 MΩ cm and all reagents not specified were Merck, GR. Solution temperature was maintained at 25 °C with an accuracy of 0.1 °C by means of a water thermostat (Haake DC3 andK20).

Morphologies of all deposits were examined by a field emission scanning electron microscope (FE-SEM, Hitachi S-4700). The composition of certain samples polarized at −0.8 V in chloride-containing electrolytes was also analyzed by this FE-SEM coupled with an energy-dispersive spectroscope (EDS). The average crystal size of Bi grains and the preferred orientation ratio are determined from the X-ray diffraction patterns measured by an X-ray diffractometer (Cu Kα, Ultima IV, Rigaku). The average surface roughness factor (denoted as Ra) of the deposits was determined via an atomic force microscope (AFM, Ben Yuan CSPM 5500).

Table 1
The preparation conditions for four BFEs with the microstructure variation in the mean grain size, preferred orientation ratio, and roughness factor (Ra).

Sample	A	B	C	D
pH	4	4	4	4
Current density (mA cm^{-2})	3	30	30	3
PEG concentration (mM)	20	100	20	100
Temperature (°C)	25	25	50	50
Stirring rate (rpm)	160	160	160	160

3. Results and discussion

Table 1 shows the electroplating conditions for preparing the Cu/Ni/Bi electrodes (BFEs) with variations in the grain size, preferred orientation ratio, and Ra of Bi in order to illustrate the influences of microstructures on the Sn-sensing activity. How to control the microstructure of Bi deposits needs to refer to our previous work [26,27], which is out of the scope of this study. Table 2 shows the dependence of the Sn^{2+}-sensing current on four BFEs with differences in the average grain size, preferred orientation ratio, or Ra of Bi deposits. Here, the crystal size of Bi grains was estimated through facet Bi(0 1 2) at 27.3° from the full width at half-maximum method [26,27,29] (see Figure S1 in the supporting information). The preferred orientation ratio, *f*, is defined as the diffraction intensity ratio of facets Bi(1 1 0) and Bi(0 1 2) [27]:

$$f = \frac{\mathrm{Bi}(1\,1\,0)}{\mathrm{Bi}(0\,1\,2)} = \frac{I_{39.7^\circ}}{I_{27.3^\circ}} \quad (1)$$

where *I* indicates the XRD peak intensity. Based on our previous work [27], *f* of Bi can be effectively controlled through means of the experimental design strategies. Ra of Bi deposits was determined by an AFM at 3 random places (10 μm × 10 μm, see Figure S2 in the supporting information). Clearly, samples A and B in Table 2 show very similar *f* and Ra values. Consequently, the effect of grain size on the sensing ability of Sn^{2+} can be compared. Similarly, the influences of the preferred orientation ratio and Ra can be demonstrated by comparing the Sn^{2+}-sensing ability of samples A and C as well as samples C and D, respectively although the grain size of Bi for sample D is larger than that for sample C (see below). Note that the surface morphology of Bi deposits, examined from the SEM images in Fig. 1, is strongly dependent upon their preferred orientation ratio. Samples A and B with a relatively high *f* value show the flower-like structure (see Fig. 1a and b), whereas a prickly rod-like shape is obtained for sample D with a low *f* value (see Fig. 1d). The above results indicate the effective control of the Bi microstructures by varying the electroplating conditions employed in this work.

In this work, the square-wave anodic stripping voltammetry (SWASV) is used to ascertain which microstructure significantly affects the Sn^{2+}-sensing ability of Bi since the SWASV does not need to remove dissolved oxygen in the analyte during the stripping analysis [19]. Curves a–d in Fig. 2 show the typical SWASV

Table 2
Four BFEs with the microstructure variation in the mean grain size, preferred orientation ratio, and roughness factor (Ra) as well as the corresponding current density of Sn^{2+} sensing.

Sample	Grain size (nm)	*f*	Ra[a] (nm)	*j* (μA cm^{-2})
A	28.98	0.48	39.34	22.7
B	35.92	0.48	40.86	59.7
C	31.46	0.11	37.43	5.51
D	38.51	0.09	71.64	~0

[a] Ra is measured by AFM through the tapping mode.

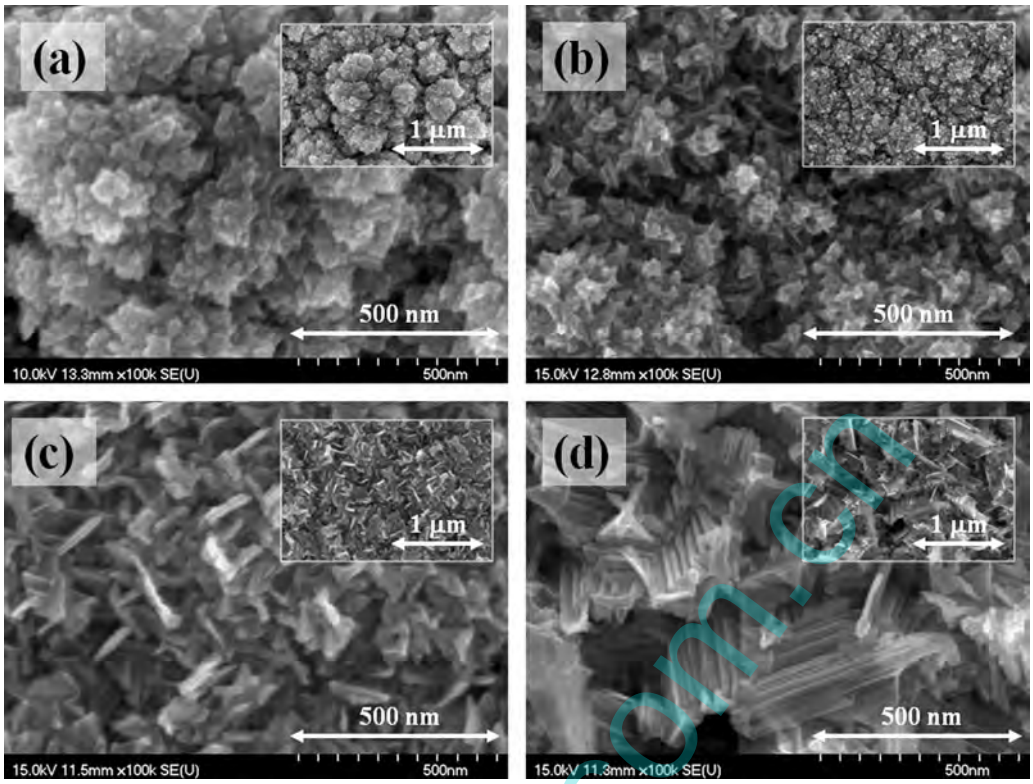

Fig. 1. The FE-SEM photographs for BFEs (a) A, (b) B, (c) C, and (d) D.

responses of Sn stripping for samples A–D, respectively, where the pre-deposition and stripping of Sn were carried out in the 0.1 M CA solution containing 2 ppm Sn^{2+} with pH = 2. From an examination of Fig. 2, the peaks centered at ca. −0.48 V on curves a and b are attributed to the anodic stripping responses of Sn pre-deposited onto the BFEs during the electrowinning step. In addition, the order of BFEs with respect to decreasing the peak current density is sample B (59.7 μA cm^{-2}) > A (22.7 μA cm^{-2}) > C (1.51 μA cm^{-2}) ≈ D (∼0 μA cm^{-2}). Note that a high *f* value is a necessary requirement for BFEs with a good sensing activity to Sn^{2+} because the influence of grain size and Ra of Bi deposits becomes negligible and no sensing current is visible when the *f* values are equal to or lower than 0.11. This statement is further supported by the fact that the increase in both grain size (a comparison of curves a and b) and *f* (a comparison of curves a and c as well as curves b and c) exhibit positive enhancements in the sensing current density from comparisons among samples A–C in Table 2 while the grain size effect is negligible when *f* is equal to/below 0.11.

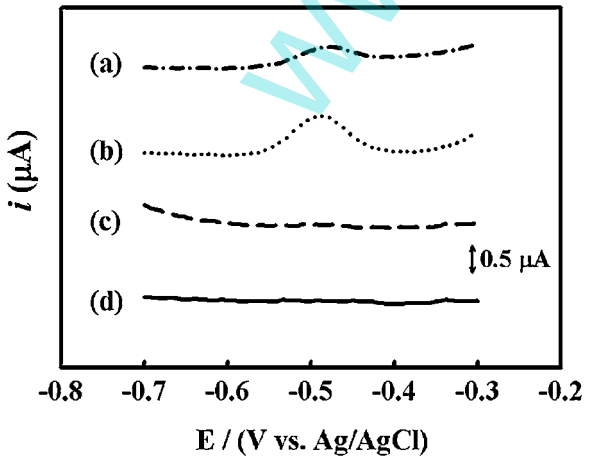

Fig. 2. The SWASV curves measured in a 0.1 M citric acid solution containing 2 ppm Sn^{2+} for BFEs (a) A, (b) B, (c) C, and (d) D.

Two possible reasons are proposed to be responsible for the strong influence of the preferred orientation ratio of Bi on the Sn^{2+}-sensing ability of BFEs. First, certain crystalline facets of metallic Bi and Sn may match each other [30]. If this is the case, the electrowinning deposition of metallic Sn atoms onto Bi grains is similar to the epitaxy growth of Sn onto Bi (e.g., Sn epitaxy growth on Bi(1 1 0) at large *f* values). Second, some crystalline facets of Bi (e.g., Bi(1 1 0)) may be favorable for depositing Sn, resulting in a higher activity on sensing Sn^{2+}. This property, different from the epitaxy deposition of Sn, depends on the surface charge of BFEs. In other words, the metallic bonding among Bi surface atoms becomes stronger at a more positive surface charge which is unfavorable for Sn deposition [31]. On the other hand, the above two reasons indicate that a larger grain of Bi is more favorable for the epitaxy growth or preferred deposition of Sn atoms on certain facets. In addition, these two possible reasons indicate that Sn^{2+} sensing does not follow the mechanism of forming Bi-based amalgams commonly found in the process of simultaneous electrowinning of Bi and heavy metal ions [30].

In order to clarify the above inferences, the XRD patterns of samples B and C pre-depositing with Sn as well as the standard patterns of Bi (#PDF 85-1330) and Sn (#PDF 04-0673) are shown in Fig. 3. For a comparison purpose, the XRD pattern of the Cu/Ni substrate is also shown in Fig. 3. Note that in order to obtain the diffraction peaks of Sn, the Sn^{2+} concentration for pre-plating Sn onto the surface of BFEs for the XRD analysis is 0.2 M. From a comparison of patterns 1–3 in Fig. 3, the much stronger and clearer diffraction peaks on patterns 2 and 3 reveal the good crystallinity of metallic Bi and Sn deposits. From the standard pattern of Sn, the order of diffraction peaks with respect to decreasing the diffraction intensity is Sn(2 0 0) > Sn(1 0 1) > Sn(2 1 1) ≫ Sn(220).

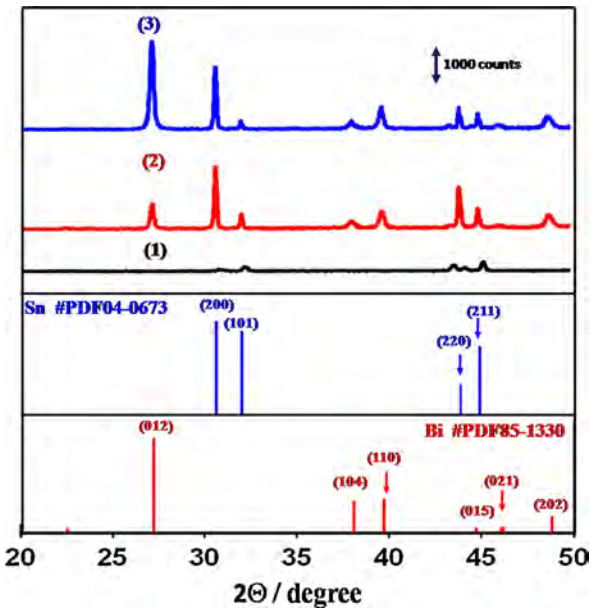

Fig. 3. The XRD patterns of (1) a Cu/Ni substrate, (2) BFE B, and (3) BFE C where BFEs B and C have been pre-deposited with Sn at −0.8 V for 300 s from a bath containing 0.2 M Sn^{2+}. The standard patterns of Bi and Sn metals are shown for comparison purposes.

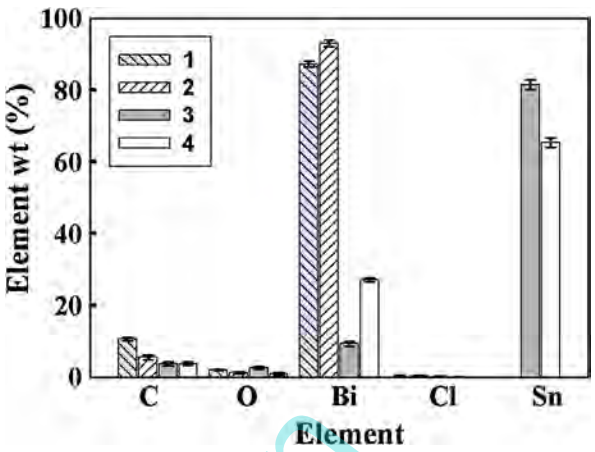

Fig. 4. The EDS results of BFEs (1,3) B and (2,4) C polarized at −0.8 V for 300 s in an aqueous solution containing (1,2) 0.4 M NaCl and (3,4) 0.2 M $SnCl_2$.

This order, however, is different from that of Sn on sample B (i.e., Sn(2 0 0) > Sn(2 2 0) > Sn(2 1 1) ≈ Sn(1 0 1)) and C (i.e., Sn(2 0 0) ≫ Sn(1 0 1) ≈ Sn(2 2 0) ≈ Sn(2 1 1)), implying the significant influence of the preferred orientation ratio of Bi on the crystallization and growth of Sn atoms electroplated from Sn^{2+}. From an examination of Fig. 2 and 3, the higher intensity of Bi(0 1 2) for sample C shows a lower Sn^{2+} sensing ability. This result indicates that the more exposure of Bi(0 1 2) will inhibit the

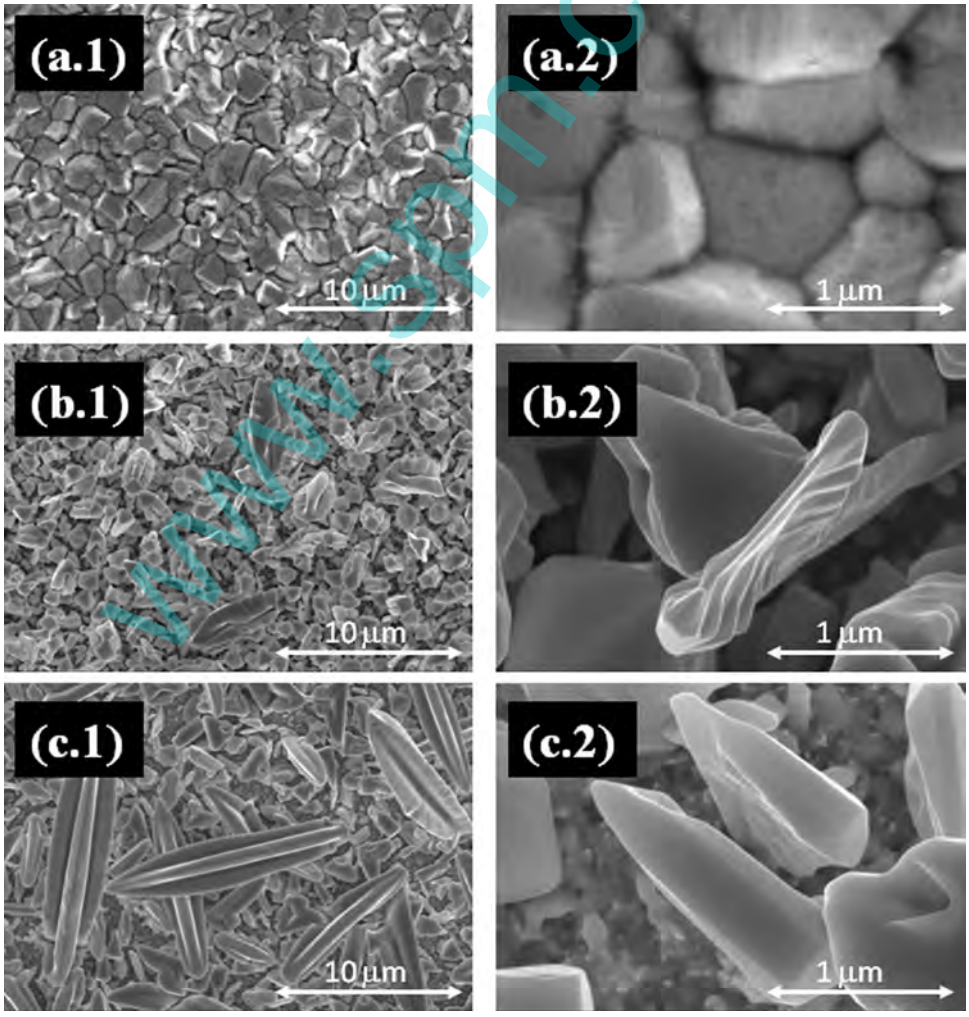

Fig. 5. The FE-SEM photographs of Sn deposits on (A) a Cu/Ni substrate, (B) BFE B, and (C) BFE C under the magnification of (1) 5k and (2) 50k.

tin deposition on the BFE, leading to a change in the morphology of tin deposited on the BFE (see below).

Note that from the standard XRD patterns of Bi and Sn, no Bi facet matches the Sn facet, disagreeing the epitaxy growth of Sn onto Bi(1 1 0). On the other hand, chloride ions from $SnCl_2$ (the precursor) might adsorb on certain Bi facets (e.g., Bi(0 1 2)) and shield the sensing ability of these fecets since some reports proposed that chloride ion could react with Bi to form bismuth oxyhalide in the positive potential region [32]. However, the Cl^- adsorption on Bi surface was investigated in organic media [33], which may be not suitable for this aqueous case. Since the pre-deposition of Sn atoms is performanced in an aqueous $SnCl_2$ solution at a very negative potential (−0.8 V vs. Ag/AgCl) at pH = 2, the selective adsorption of chloride ion onto certain Bi facets shoud not occur because of the electrostatic force. In order to confirm this idea, the energy-dispersive spectroscopic (EDS) analysis is employed to detect the element distribution on samples B and C which were polarized at -0.8 V for 300 seconds in two aqueous solutions containing 0.4 M NaCl and 0.2 M $SnCl_2$, respectively. The EDS results are summarized in Fig. 4. Based on the EDS results of samples B and C in NaCl (i.e., bars 1 and 2, respectively), the chloride content on samples B and C is almost undetectable due to the fact that the chloride content on both BFEs is close to the detecting limit. The same results are obtained when both BFEs were polarized in the $SnCl_2$ solution, supporting that chloride ion does not selectively adsorb on certain facets of Bi deposits in the negative potential region. Also note that the Sn content on sample B (81.5 wt%) is higher than that on sample C (65.3 wt%) although both BFEs were polarized under identical conditions. This result indicates a thicker Sn deposit on sample B in comparison with that on sample C. Therefore, the rate of Sn deposition onto sample B (with a higher *f* value) is faster than that on sample C (with a lower *f* value). Based on all the above results and discussion, the growth of Bi(1 1 0) crystalline facet is favorable for depositing Sn, leading to the significant enhancement in the Sn^{2+}-sensing activity of metallic Bi films. In addition, the Sn^{2+}-sensing behavior on BFEs does not follow the mechanism of forming amalgams of Bi alloys in the pre-deposition period.

Clearly, the procedure of Sn^{2+} detection on BFEs can be qualitatively divided into two steps: (i) the pre-concentration and (ii) anodic stripping of pre-deposited Sn atoms. In the first step, Sn^{2+} is reduced to form metallic Sn atoms onto the surface of Bi grains with high exposure of Bi(1 1 0) (at −0.8 V in this work). In the following stripping step, the pre-deposited Sn atoms are oxidized and dissolved into the stripping solution (by means of the SWASV in this work).

The uniform dispersion and microstructures of Sn on the Cu/Ni substrate and the BFEs are clearly visible from the SEM images shown in Fig. 5. Again, the Sn^{2+} concentration for plating Sn onto the surface of BFEs for the morphology examination is 0.2 M. The chunk-like tin metal is formed on the Cu/Ni substrate (see Fig. 5A), whereas metallic Sn with a triangle-like shape is obtained on samples B and C (see Fig. 5B and C). This result reveals that the surface morphology of Sn pre-deposits can be changed by varying the substrate (e.g., changing from Ni to Bi films here). More importantly, the morphologies of tin deposits on samples B and C are different. The above results further support the significant influence of the Bi surface morphology resulting from the variation in the preferred orientation ratio of Bi grains on the crystallization and growth of Sn atoms plated from Sn^{2+}.

Since sample B shows the highest sensing current of Sn^{2+}, a further increase in the *f* value to 0.89 of a BFE is done through the statistical strategy and its sensing ability is examined by changing the Sn^{2+} concentration from 0.2 to 95 ppm in the testing solution. Typical SWASV results are shown in Fig. 6A and the plot for the peak current against the Sn^{2+} concentration is shown as inset in Fig. 6A. The linear dependence of the SWASV peak current on the Sn^{2+} concentration reveals the good sensitivity of this BFE. The linear dependence can be perfectly fitted by the following equation:

$$i = 1.31C + 1.51 \quad (R^2 = 0.957)$$

where *i* and *C* indicate the peak current (in μA) and Sn^{2+} concentration (in ppm), respectively. The above results reveal that this new BFE is a good electrode for Sn^{2+} sensing with concentration varying from 0.2 to 95 ppm.

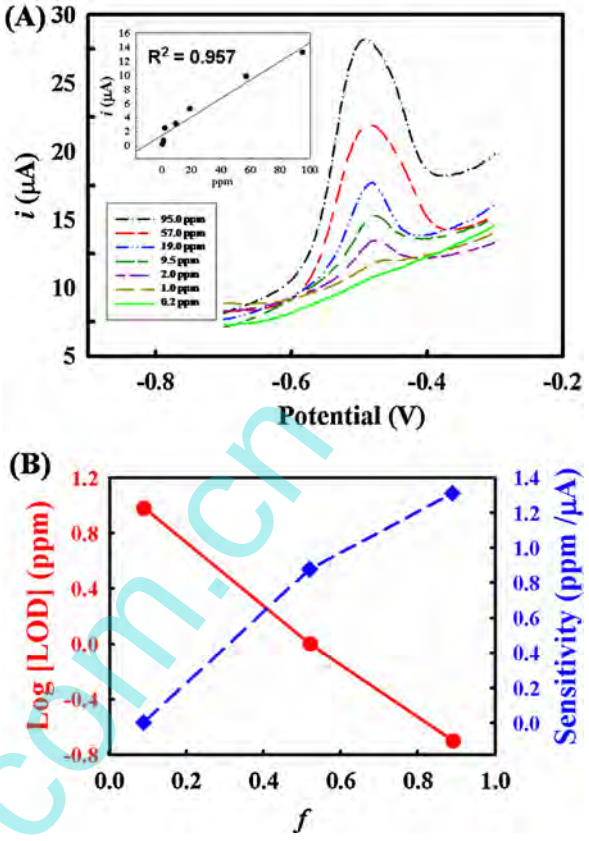

Fig. 6. (A) SWASV curves measured in 0.1 M citric acid for a BFE with *f* = 0.89 with the Sn^{2+} concentration varying from 0.2 to 95 ppm. Inset shows the calibration curve for the SWASV peak current against the Sn^{2+} concentration. (B) Dependence of the limit of detection (LOD, dot) and the sensitivity (slope of calibration curves, square) on *f* of BFEs. The average grain size is 48.9, 27.7, and 27.0 nm when the *f* values of BFEs are equal to 0.09, 0.52, and 0.89, respectively.

Fig. 6B shows the increase in the Sn^{2+} sensitivity on the *f* value (from 0.05 to 0.89) of BFEs although the average crystal size of Bi grains is 48.9, 27.7, and 27.0 nm when the *f* values of BFEs are equal to 0.09, 0.52, and 0.89, respectively. In addition, the limit of detection (LOD) concentration of Sn^{2+} on BFEs is promoted by increasing the *f* value of Bi deposits. The monotonous enhancements in the Sn^{2+} sensitivity and LOD with increasing the *f* value of Bi deposits further support the conclusion that the exposure of Bi(1 1 0) crystalline facet is the main key factor determining the Sn^{2+}-sensing ability of BFEs. This finding emphasizes that the pre-deposition of Sn on Bi does not follow the mechanism of forming Bi-based amalgams. In addition, from the comparison of samples A–C in Table 2, a synergistic effect between the increase in grain size and *f* value has been found to enhance the current density of Sn^{2+} sensing when the *f* value is relatively large (e.g., *f* = 0.48 in Table 2). The next step to further increase the detection ability of BFEs for Sn^{2+} sensing is to enlarge the crystal size but maintain a high *f* value of Bi grains for BFEs, which is under study now.

4. Conclusions

The Sn^{2+}-sensing ability of BFEs has been found to strongly depend on the preferred orientation ratio of Bi deposits, reasonably attributed to that the Bi(1 1 0) facet is favorable for Sn deposition. A synergistic effect between grain size and f on enhancing the Sn^{2+}-sensing ability is obtained when f is relatively large (e.g., $f \sim 0.48$). A BFE with a f value = 0.89 show good Sn^{2+} sensing with the Sn^{2+} concentration varying from 0.2 to 95 ppm. This investigation also emphasizes that the step of pre-depositing Sn on Bi for Sn^{2+} sensing does not follow the mechanism of forming Bi-alloy amalgams. Accordingly, the crystallization and growth of Sn atoms plated from Sn^{2+} are significantly influenced by changing the Bi surface morphology resulting from the variation in the preferred orientation ratio of Bi grains.

Acknowledgement

The financial support from NSC-Taiwan and the boost program in LCERC of NTHU is gratefully acknowledged.

Appendix A. Supplementary data

Supplementary data associated with this article can be found, in the online version, at http://dx.doi.org/10.1016/j.electacta.2013.04.121.

References

[1] J. Wang, Analytical Electrochemistry, 2nd ed., Wiley, New York, 2000.
[2] E.A. Hutton, B. Ogorevc, S.B. Hočevar, F. Weldon, M.R. Smyth, J. Wang, An introduction to bismuth film electrode for use in cathodic electrochemical detection, Electrochemistry Communications 3 (2001) 707.
[3] A. Economou, P.R. Fielden, Mercury film electrodes: developments, trends and potentialities for electroanalysis, Analyst 128 (2003) 205.
[4] S. Legeai, S. Bois, O. Vittori, A copper bismuth film electrode for adsorptive cathodic stripping analysis of trace nickel using square wave voltammetry, Journal of Electroanalytical Chemistry 591 (2006) 93.
[5] J. Wang, J.M. Lu, S.B. Hocevar, P.A.M. Farias, B. Ogorevc, Bismuth-coated carbon electrodes for anodic stripping voltammetry, Analytical Chemistry 72 (2000) 3218.
[6] J. Wang, Stripping analysis at bismuth electrodes: a review, Electroanalysis 17 (2005) 1341.
[7] I. Švancara, K. Vytřas, Electroanalysis with bismuth electrodes: state of the art and future prospects, Chemicke Listy 100 (90–113) (2006).
[8] A. Economou, Bismuth-film electrodes: recent developments and potentialities for electroanalysis, Trends in Analytical Chemistry 24 (2005) 334.
[9] A.P. Periasamy, S. Yang, S.M. Chen, Preparation and characterization of bismuth oxide nanoparticles-multiwalled carbon nanotube composite for the development of horseradish peroxidase based H_2O_2 biosensor, Talanta 87 (2011) 15.
[10] Y.-D. Tsai, C.-C. Hu, C.-C. Lin, Electrodeposition of Sn–Bi lead-free solders: effects of complex agents on the composition, adhesion, and dendrite formation, Electrochimica Acta 53 (2007) 2040.
[11] C. Prior, G.S. Walker, The use of the bismuth film electrode for the anodic stripping voltammetric determination of tin, Electroanalysis 18 (2006) 823.
[12] G. Yang, Y. Wang, F. Qi, Differential pulse anodic stripping voltammetric determination of traces of tin using a glassy carbon electrode modified with bismuth and a film of poly(bromophenol blue), Microchimica Acta 177 (2012) 365.
[13] C. Prior, Anodic stripping voltammetry of tin at the bismuth film electrode using cetyltrimethylammonium bromide, Electroanalysis 22 (2010) 1446.
[14] X. Jiang, Q. Sun, J. Zhang, B. Wang, X. Du, Determination of Sn^{2+} ion in canned foods using bismuth- and antimony-film electrodes, Sensor Letters 7 (2009) 97.
[15] M. Frena, I. Campestrini, O.C.d. Braga, A. Spinelli, In situ bismuth-film electrode for square-wave anodic stripping voltammetric determination of tin in biodiesel, Electrochimica Acta 56 (2011) 4678.
[16] S. Blunden, T. Wallace, Tin in canned food: a review and understanding of occurrence and effect, Food and Chemical Toxicology 41 (2003) 1651.
[17] M. Hoch, Organotin compounds in the environment — an overview, Applied Geochemistry 16 (2001) 719.
[18] V. Mirceski, S.B. Hocevar, B. Ogorevc, R. Gulaboski, I. Drangov, Diagnostics of anodic stripping mechanisms under square-wave voltammetry conditions using bismuth film substrates, Analytical Chemistry 84 (2012) 4429.
[19] F. Arduini, J.Q. Calvo, A. Amine, G. Palleschi, D. Moscone, Bismuth-modified electrodes for lead detection, Trends in Analytical Chemistry 29 (2010) 1295.
[20] E.A. Hutton, S.B. Hocevar, L. Mauko, B. Ogorevc, Bismuth film electrode for anodic stripping voltammetric determination of tin, Analytica Chimica Acta 580 (2006) 244.
[21] H. Xu, L. Zeng, D. Huang, Y. Xian, L. Jin, A Nafion-coated bismuth film electrode for the determination of heavy metals in vegetable using differential pulse anodic stripping voltammetry: an alternative to mercury-based electrodes, Food Chemistry 109 (2008) 834.
[22] L. Jiang, Y. Wang, J. Ding, T. Lou, W. Qin, An ionophore–Nafion modified bismuth electrode for the analysis of cadmium(II), Electrochemistry Communications 12 (2010) 202.
[23] C. Kokkinos, A. Economou, I. Raptis, C.E. Efstathiou, T. Speliotis, Novel disposable bismuth-sputtered electrodes for the determination of trace metals by stripping voltammetry, Electrochemistry Communications 9 (2007) 2795.
[24] L. Baldrianova, I. Svancara, S. Sotiropoulos, Anodic stripping voltammetry at a new type of disposable bismuth-plated carbon paste mini-electrodes, Analytica Chimica Acta 599 (2) (2007) 249.
[25] A. Bobrowski, A. Królicka, J. Zarębski, Morphology and electrochemical properties of the bismuth film electrode ex situ electrochemically plated from perchloric acid, Electroanalysis 22 (2010) 1421.
[26] Y.D. Tsai, C.H. Lien, C.C. Hu, Effects of polyethylene glycol and gelatin on the crystal size, morphology, and Sn^{2+}-sensing ability of bismuth deposits, Electrochimica Acta 56 (2011) 7615.
[27] C.H. Lien, C.C. Hu, Y.D. Tsai, D.S.H Wang, Preferred orientation control of Bi deposits using experimental strategies, Journal of the Electrochemical Society 159 (2012) D260.
[28] Y.D. Tsai, C.C. Hu, Composition control of Sn–Bi deposits: interactive effects of citric acid, ethylenediaminetetraacetic acid, and poly(ethylene glycol), Journal of the Electrochemical Society 156 (2009) D490.
[29] A. Jankowski, J. Hayes, R. Smith, B. Reed, M. Kumar, J. Colvin, Grain growth in bismuth coatings, Materials Science and Engineering A 431 (2006) 106.
[30] B. Cao, Y. Li, G. Duan, W. Cai, Growth of ZnO nanoneedle arrays with strong ultraviolet emissions by an electrochemical deposition method, Crystals Growth and Design 6 (2006) 1091.
[31] K. Lust, M. Väärtnõu, E. Lust, Adsorption of halide anions on bismuth single crystal plane electrodes, Electrochimica Acta 45 (2000) 3543.
[32] S.K. Poznyak, A.I. Kulak, Electrochemical formation of bismuth oxyhalide films in neutral halide solutions, Journal of Electroanalytical Chemistry 278 (1990) 227.
[33] M. Väärtnõu, E. Lust, Impedance study of chloride ions adsorption on Bi(1 1 1) and Bi(0 1 1) single crystal planes in ethanol, Journal of Electroanalytical Chemistry 578 (2005) 273.